


## RESEARCH ARTICLE

# Effect of load reduction mechanisms on loads and blade bearing movements of wind turbines

Matthias Stammler<sup>1</sup>  | Philipp Thomas<sup>1</sup> | Andreas Reuter<sup>1,2</sup> | Fabian Schwack<sup>2</sup> | Gerhard Poll<sup>2</sup>

<sup>1</sup>Fraunhofer-Institute for Wind Energy Systems, Bremerhaven, Germany

<sup>2</sup>Institut für Maschinenkonstruktion und Tribologie (IMKT), Leibniz University Hannover, Hanover, Germany

**Correspondence**

Matthias Stammler, Fraunhofer IWES, Am Schleusengraben 22, 21029 Hamburg, Germany.

Email: matthias.stammler@iwes.fraunhofer.de

**Funding information**

Bundesministerium für Wirtschaft und Energie, Grant/Award Number: 0325918A; German Federal Ministry for Economic Affairs and Energy

**Abstract**

The power control of wind turbines is usually realized via a change in the pitch angle of the rotor blades. Pitching facilitates the exact control of the turbines and the reliable deceleration of the rotor when required. Pitch movements can moreover be used for load control. One of these methods is called individual pitch control (IPC). IPC controls the blades individually and brings about a significant reduction in the fatigue loads and extreme loads placed on the structural components, while at the same time reducing the yield of the turbine only slightly. The lower loads reduce material costs, and thus, the cost of energy (CoE) is reduced, despite the slight reduction in yield. The method is nevertheless not used everywhere since the additional movement cycles put the rotor blade bearings in particular under stress. Special attention must be paid to small amplitude oscillating movements, which carry a high risk of inducing surface damage in the rolling contacts of the blade bearings. This paper uses a cycle analysis of the IWT7.5-164 reference turbine to illustrate the differences in the movement patterns of wind turbine blade bearings with and without IPC. Moreover, model calculations with single contacts are used to show which of the movement patterns carries a risk of inducing surface damage. The use of IPC leads to the expected load reduction at the blade root. In current literature, IPC is usually assumed to have a negative influence on the life expectancy of blade bearings, but the findings of this study contradict this. The summed blade bearing movement is increased, although the number of very small pitch angles occurring is reduced. This reduction reduces the risk of wear in the blade bearings.

**KEYWORDS**

Blade Bearing, Individual Pitch Control, Rolling contact fatigue, Slewing Bearing, Wear

## 1 | INTRODUCTION

With a small number of exceptions, wind turbines for electricity generation use the lift principle to convert the energy contained in the wind into the rotational energy of a shaft that drives a generator. The profile geometry of the rotor blades is designed to have the best possible ratio of lift to drag across the broadest range of wind speeds possible in order to efficiently convert the power of the wind.<sup>1</sup> At the same time, structural

-----  
This is an open access article under the terms of the Creative Commons Attribution-NonCommercial License, which permits use, distribution and reproduction in any medium, provided the original work is properly cited and is not used for commercial purposes.

© 2019 The Authors. Wind Energy published by John Wiley & Sons Ltd

requirements need to be fulfilled, and they often require larger profile thicknesses than are required for purely aerodynamic reasons. While the first commercial wind turbines used the effect of stall at higher wind speeds to limit the power, blade angle adjustment (pitching) has been used almost exclusively for several decades to control the power. This not only facilitates more precise control at the nominal operating point but also reduces the structural loads when the wind turbine is switched off and allows it to start up at low wind speeds.<sup>2</sup>

Pitch controllers do not only allow the power of the turbine to be controlled, however. Since safety reasons dictate that they are always designed so as to be redundant and mutually independent, the pitch angles of the individual rotor blades can be adjusted individually as well.<sup>3</sup> This can be used to reduce load peaks of individual blades by relatively small and short pitch movements or to harmonize the loads of all three rotor blades. The method, termed individual pitch control (IPC), can be designed for different control variables. In addition to the individual blade root loads, it is possible to minimize certain rotor moments.<sup>4</sup> Depending on the design of the controllers, which also depends on the site conditions, IPC can be used to reduce fatigue loads and extreme loads.<sup>5</sup> When loads that are the drivers for the design of structures are reduced, these structures can be designed to be lighter and lower cost, thus reducing the capital costs of the wind turbine. IPC reduces not only the loads but also the amount of electricity generated, but this is an acceptable disadvantage compared with the advantages that can be achieved.<sup>4</sup>

The rotor blade bearings used in practice are usually rolling bearings, most commonly four-point contact bearings.<sup>6</sup> Replacing damaged bearings entails significant costs, because at least one rotor blade has to be removed. If rolling bearings rotate constantly under constant or almost constant loads and speeds, the lubricant can form a film that separates the rolling elements from the raceway. In this case, hardly any surface wear occurs and fatigue is the dominating damage mechanism.<sup>7,8</sup> The relatively small, oscillating pitch movements with amplitudes of a few degrees that are executed by the IPC controllers often do not lead to the formation of a separating lubricating film, and rolling elements and bearing raceway come into direct contact, which can result in adhesive and abrasive wear.<sup>9-11</sup>

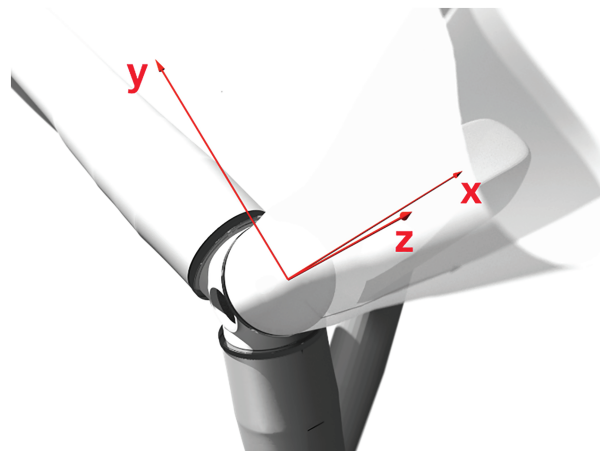
Many versions of the control algorithms for the use of IPC have been developed and assessed in recent years.<sup>12</sup> There has so far been hardly any assessment of the impact of using these algorithms on the mechanical components of the pitch system, ie, drive and rotor blade bearings, however. It is generally assumed that they will simply be subject to greater strain.<sup>12,13</sup> It is relatively easy to test the drives, and they can be replaced with relative ease should they fail. There are currently no meaningful methods for calculating the service life of rotor blade bearings that are subjected to oscillations with small pitch angles, however.<sup>14-17</sup> Test methods used to date have been limited to the implementation of friction moment tests<sup>18,19</sup> and tests for rolling contact fatigue.<sup>19</sup> Methods for the long-term testing of mechanisms that induce damage on the surface are still under development.<sup>20</sup> Moreover, it is currently not possible to calculate wear as it is forming and evolving.<sup>21</sup> The probability that it will occur can be assessed with the aid of the operating conditions, particularly the kinematic parameters and the loads, however.<sup>22</sup>

This paper shows the impact of using IPC on the loads and the movement patterns of the rotor blade bearings using the example of the IWT-7.5-164 reference wind turbine. The probabilities that damage is induced on the surface are assessed for both modes of operation. To this end, the reference turbine and the methods used for the load simulation, movement pattern analysis, and rolling contact simulation are first presented in Section 2. Section 3 then contains the corresponding results and a discussion thereof; the conclusion follows in Section 4.

## 2 | REFERENCE TURBINE, SIMULATION, AND DATA ANALYSIS

### 2.1 | Reference coordinate system

The reference system of the blade root is shown in Figure 1. The local reference system is a Cartesian coordinate system that rotates with the rotor. Its origin is at the blade root. The z-axis points along the rotor blade axis and the y-axis points in the rotation direction of the blade.



**FIGURE 1** Reference coordinate system of the blade root [Colour figure can be viewed at [wileyonlinelibrary.com](http://wileyonlinelibrary.com)]



## 2.2 | Blade bearing

A blade bearing was designed for the IWT-7.5-164,<sup>23</sup> as described in Schwack et al.<sup>24</sup> The bearing is a double-row four-point contact bearing with a nominal diameter of 4690 mm, a ball diameter of 80 mm, and 147 balls per row. Four-point contact bearings are in widespread use as blade bearings. Figure 2 shows a section view of the bearing with the major dimensions. The blade connects to the inner ring of the bearing. The bearing friction was not included in the HAWC2<sup>25</sup> load simulations because no reliable computational models are currently available for the friction of rotor blade bearings.<sup>18</sup>

## 2.3 | Reference turbine IWT-7.5-164 and simulation

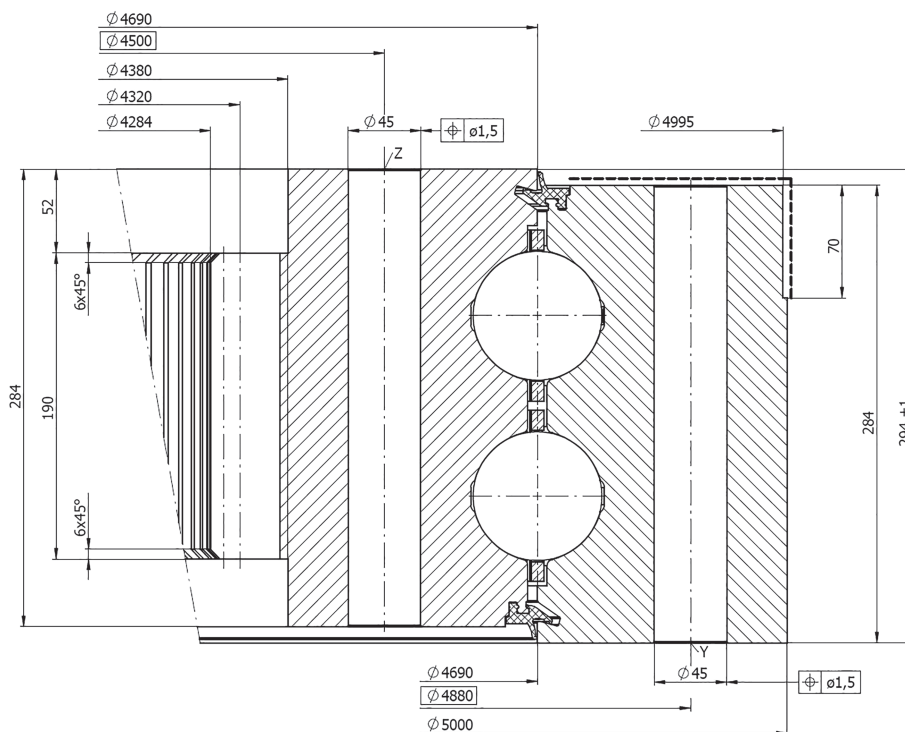
The IWES wind turbine IWT-7.5-164<sup>23</sup> is a wind turbine with a rotor diameter of 164 m, a hub height of 119.3 m (hybrid tower), and a total mass of approximately 2000 t. It combines a relatively low specific power and a detailed blade design with a control strategy designed for load reduction. The wind turbine was developed for sites near the coast with high average wind speed and turbulence intensity (IEC A1) to consider worst-case load scenarios in the design. This means that various concepts for the passive and active load reduction can be investigated. Within this work, the aeroelastic code HAWC2<sup>25</sup> is used to simulate IEC load cases. HAWC2 has been developed by the Wind Energy department of the Technical University of Denmark in Copenhagen.

Table 1 lists important characteristics of the IWT-7.5-164.

### 2.3.1 | Turbine pitch angle and generator torque control

The Fraunhofer IWES baseline controller<sup>23</sup> for pitch-regulated, variable-speed wind turbines features both collective pitch control and individual pitch control capabilities including partial-loading and full-loading operating modes. The IPC adds a pitch angle to the collective pitch angle if this collective pitch angle reaches values larger than  $2.3^\circ$  in both the partial-loading and full-loading regions. The controller uses the blade pitch angles and the electromagnetic generator torque to control the wind turbine. The maximum permissible pitch speed of the controller is  $6^\circ$  per second. The basic supervisory control functions include normal stop, emergency stop, overspeed monitor, and grid loss.

The individual pitch controller takes the current collective pitch angle set point as a mean value and adds an individual zero-mean pitch offset for each blade. The individual pitch angles at the three blades are calculated from the measured blade root bending moments to compensate for the 1P asymmetrical out-of-plane loads on the rotor in tilt and yaw directions produced by the inhomogeneity of turbulence, wind shear, yaw



**FIGURE 2** Section view of the blade bearing with major dimensions

**TABLE 1** Important characteristics of IWT-7.5-164 [Colour table can be viewed at wileyonlinelibrary.com]

Property		Value
Rated generator power	$P_r$	7.5 MW
Wind class		IEC A1
Hub height	$h_{hub}$	119.3 m
Rotor diameter (unconed)	$D_{rotor}$	164 m
Rotor blade length (along pitch axis)	$l_{blade}$	80 m
Specific power (per swept area)	$\psi_{rotor}$	355 W/m <sup>2</sup>
Cut-in wind speed	$V_{in}$	3 m/s
Rated wind speed	$V$	11 m/s
Cut-out wind speed	$V_{out}$	25 m/s
Minimum rotational speed	$\Omega_{min}$	5 rpm
Rated rotational speed	$\Omega_r$	10 rpm
Rated tip speed	$V_{tip-r}$	85.9 m/s
Design tip speed ratio	$\lambda_D$	8.4
Blade cone angle (upwind)	$\theta_{cone}$	2°
Shaft tilt angle (upwards from horizon)	$\theta_{tilt}$	5°
Total turbine efficiency	$\eta_{tot}$	95%
Drive train concept		Direct drive
Control concept		Variable speed, IPC, peak-shaver
Rotor configuration		Upwind, 3-blade
Tower mass	$m_{tower}$	1 467 355 kg
Rotor-Nacelle-Assembly mass	$m_{RNA}$	536 586 kg

misalignment, tower shadow, and aerodynamic asymmetry of the rotor, which dominate the fatigue loads of the blades and the main shaft. 1P refers to the rotor's rotational frequency.

### 2.3.2 | Modeling of the pitch drive

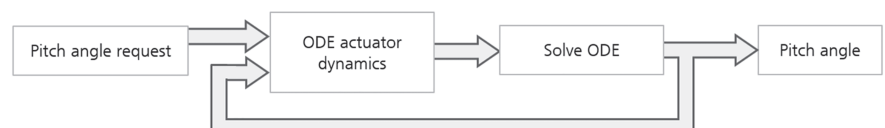
In HAWC2, the pitch drive is provided in the form of an external DLL. For the simulations carried out here, the "servo\_with\_limits.dll" model was used, which was published together with the DTU 10 MW Reference Wind Turbine.<sup>26</sup>

The pitch calculation (Figure 3) takes the demanded value of the pitch angle  $\theta_{ref}$  as the input value and uses it to calculate the actual value for the pitch angle  $y_1$  (actual control variable and output value), the pitch rate  $y_2$ , and the pitch acceleration. A temporal offset exists between the input and the output value of the pitch angle, which is generated by describing the output values with a differential equation and calculating them using a Runge-Kutta method.

$$\frac{dy_2}{dt} = -\frac{a_{max}}{V_{max}} * y_2 + a_{max} * \tanh\left(w_0^2 * \frac{\theta_{ref} - y_1}{a_{max}} - \left(2 * \beta_0 * w_0 - \frac{a_{max}}{V_{max}}\right) * \frac{y_2}{a_{max}}\right), \quad (1)$$

$$\frac{dy_1}{dt} = y_2. \quad (2)$$

Equations (1) and (2) solve for the pitch angle  $y_1$  and the pitch velocity  $y_2$ . Equation (2) computes  $y_2$  and resembles a PT1 behavior.  $y_2$  is limited by the fact that the acceleration goes into saturation. Equation (1) computes  $y_1$  and shows a PT2 behavior. The equations use the maximum pitch velocity  $v_{max}$ , the maximum pitch acceleration  $a_{max}$ , the filter frequency  $w_0$ , and the filter damping ratio  $\beta_0$ . After the differential equations are



**FIGURE 3** Schematic representation of the calculation of the pitch angle

solved, the calculated pitch angle is compared with the limit values; in case of limit violation, the pitch angle is replaced with the applicable limit value, and the pitch rate is set to zero.

## 2.4 | Load calculations

The load calculations were implemented according to the specifications of IEC-61400-1 Ed.3<sup>27</sup> with HAWC2.<sup>25</sup> The power production according to the design load case (DLC) 1.2<sup>27</sup> was simulated, which uses normal turbulence model (NTM<sup>27</sup>) from the cut-in wind speed of 3 m/s up to the cut-out speed of 25 m/s. A total of 216 simulations were carried out.

The damage equivalent loads (DELs) were determined for the 216 individual time series, each of 600-second duration, by means of rainflow counting carried out by the Matlab-based mLife tool, which was initially developed by NREL.<sup>28</sup> The occurrence of the individual simulations associated with an average wind speed is specified by the Weibull distribution. It is assumed that, over its 20-year service life, the wind turbine is in power production mode between cut-in and cut-out wind speed for 95% of the time. The simulations carried out thus reflect most of the operating time of the turbine, and a meaningful statement can be made about the operational load of the blade bearing.

## 2.5 | Damage mechanisms of blade bearings

Several types of damage can occur in rotor blade bearings of wind turbines as a result of the complex and varied loading.

Table 2 provides an overview of several selected types of damage. In order for the present paper to be concise, the focus here is put on the wear induced on the surface.

The oscillating movement between the rolling element and raceway of the blade bearing can give rise to different damage mechanisms that differ from the known damage mechanisms in rotating bearing applications. Since the focus of tribology research during the past 70 years has been on rotating rolling bearings due to their large number of applications,<sup>7</sup> little research has been conducted into the damage mechanisms in oscillating rolling bearings. General methods for calculating the thickness of the lubricating film,<sup>7,29</sup> fatigue life,<sup>30,31</sup> or the friction moment<sup>18</sup> cannot be used for oscillating rolling bearings without adjustments being made. In oscillating mode, the operating parameters such as oscillation amplitude and oscillation frequency, as well as the lubricant used, decide which of the various damage mechanisms occur. The oscillation amplitude, oscillation frequency, and the rolling element load can vary greatly, depending on the control concept of the pitch control. The comparison between IPC and CPC (collective pitch control) therefore also has an impact on the tribological conditions in the rolling bearing system.

Figure 4 shows wear that occurred in experiments on four-point contact bearings under scaled rotor blade bearing conditions after fewer than 1 000 000 cycles. In the event that wear occurs, this is the life-limiting damage for rotor blade bearings.

### 2.5.1 | Raceway fatigue


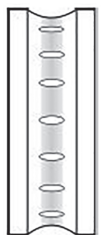

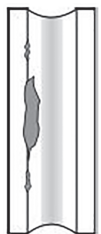

Assuming that a rolling bearing is correctly mounted, lubricated, maintained, and not overly loaded, the service life of the machine component is determined by raceway fatigue.<sup>32</sup> The thickness of the lubricating film is also important. With raceway fatigue, micro-cracks form below the surface of the raceway, where the highest material stress occurs. When the rolling elements continue to roll across these cracks, they can migrate to the surface and cause the surface of the raceway to flake. The fundamental theory of raceway fatigue in rotating rolling bearings was developed by Lundberg and Palmgren.<sup>33</sup> The estimation of the fatigue life of rotor blade bearings is complex due to the continuously changing operating parameters and the oscillating stress. Although different approaches to fatigue life exist for oscillating rolling bearings, they have not been sufficiently validated as of yet. An overview of the possible fatigue life calculations for rotor blade bearings can be found in Schwack et al.<sup>14</sup> This work applies the different methods to exemplary load cases of the IWT-7.5-164. The comparison showed significant deviations between the approaches compared. Moreover, most approaches were not available for the operating parameters given, since most of the amplitudes were not within the scope of the approaches. Furthermore, wear will occur with small oscillation amplitudes because a separating lubricating film cannot form.

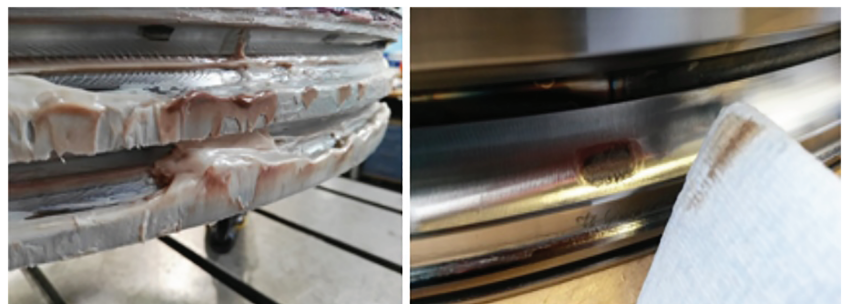
### 2.5.2 | Wear

To characterize the oscillating movements of bearings, the ratio of the distance covered  $x$  and the width of the contact area  $2b$  allows to transfer results between different bearing sizes.<sup>11</sup> Figure 5 shows examples for the  $x/2b$ -ratio.

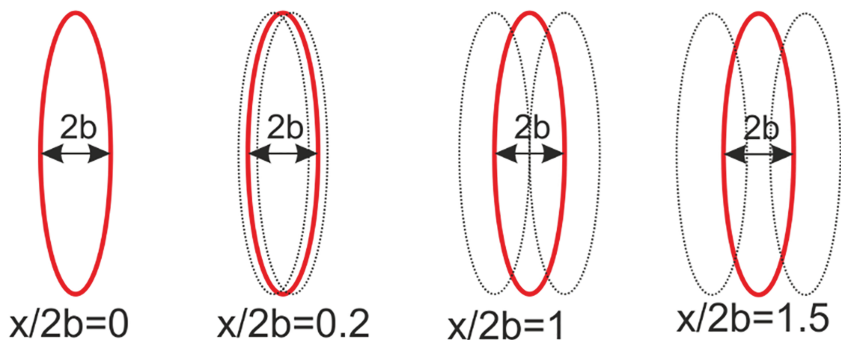
With small oscillation amplitudes ( $x/2b < 1.5$ ), mixed friction prevails in the contact.<sup>34</sup> The most common wear phenomena under oscillating movements are false brinelling and fretting corrosion. False brinelling was mentioned in the literature as early as 1937.<sup>35</sup> Damage was discovered in the wheel bearings of cars before the car was handed over to the customer. The damage was caused as the cars were being shipped by small oscillations ( $x/2b < 1$ ) between rolling element and raceway that were triggered by external vibrations. The micro-movements cause the lubricant to be pushed out of the contact, and sufficient reflow is not possible.<sup>9,36</sup> The movements between rolling element and raceway result in slight

**TABLE 2** Selected types of damage to rolling bearings

Raceway fatigue		<p>Caused by the cyclic load resulting from the rolling elements rolling over the raceway when the turbine is in operation. Can be estimated with the aid of international standards for rotating applications. The damage originates below the raceway surface.</p>
True brinelling		<p>Named for James Brinell, inventor of the Brinell hardness test. True brinelling is caused by overloading while the rolling bearing is not rotating. The overloading causes plastic deformations of the raceway.</p>
Oscillation wear		<p>Distinction between false brinelling and fretting corrosion. The damage is caused by the oscillating movement between rolling element and raceway. Mild wear in the form of false brinelling can escalate to fretting corrosion as the number of cycles increases. Fretting corrosion promotes abrasive wear through the formation of particles.</p>
Edge wear		<p>Increased loads and/or deformations lead to changes in the contact angles of the rolling bearing. The raceway edge then suffers wear. Plastic deformations and flaking off of the edges as the consequence of the edge wear.</p>
Ring fracture		<p>Consequential damage caused by bearings damaged in operation. Changes to the bearing geometry caused by fatigue or wear lead to much greater loads in the bearing. The excessive loads lead to forced fracture.</p>



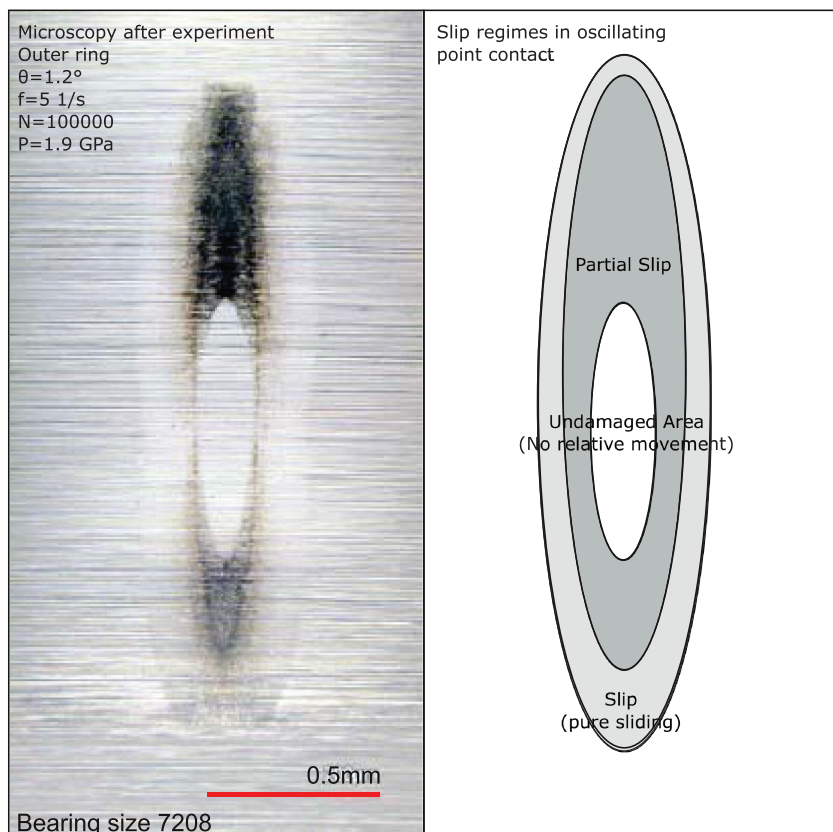
**FIGURE 4** Wear under scaled rotor blade bearing conditions [Colour figure can be viewed at [wileyonlinelibrary.com](http://wileyonlinelibrary.com)]



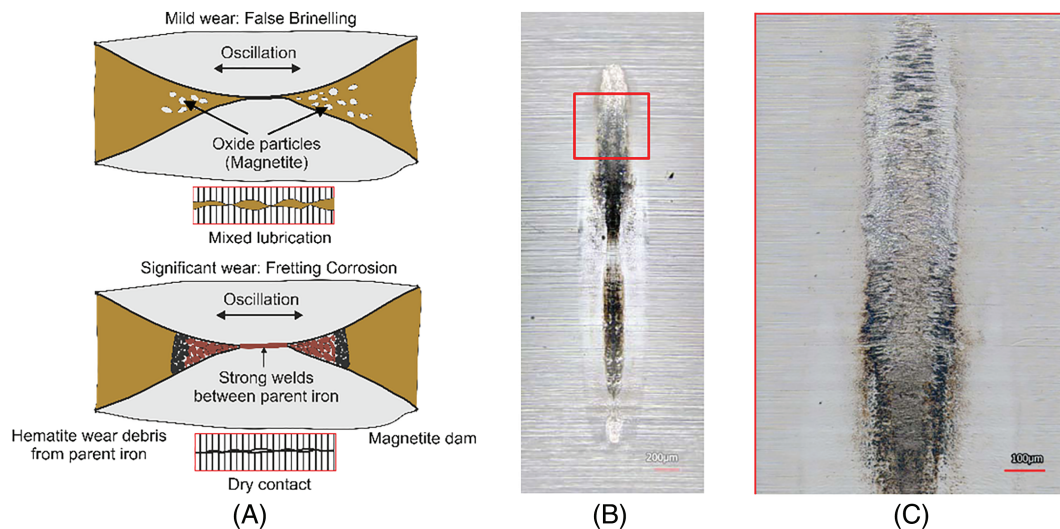
**FIGURE 5**  $x/2b$ -ratio [Colour figure can be viewed at [wileyonlinelibrary.com](http://wileyonlinelibrary.com)]

wear, which can be split up into three sections according to the kinetics for ball bearings. There is a ring-shaped area in the outer region where pure sliding prevails. This area surrounds a region in which partial sliding occurs.<sup>37</sup> These regions are subject to wear, as can be seen in Figure 6. There is furthermore a region where no relative movement occurs. A rolling movement between rolling element and raceway takes place in this region. Moreover, the tribochemical effects that occur between rolling element and raceway can be seen. In the region where slip takes place, a smoothing of the rough surface can be observed in the oscillating contact. In the region where partial slip occurs, the reaction product magnetite is also formed because the natural oxide layer is worn away.<sup>38</sup> Magnetite is formed when mixed friction predominates.

In the case where there is no lubricant in the contact, the reaction product hematite forms,<sup>38</sup> which can be easily recognized by its reddish color. With dry friction, the damage mechanism is called fretting corrosion. Fretting corrosion is characterized by very aggressive wear, which results from the dry friction and brings particles into the raceway contact. This can result in even more pronounced abrasive wear. Fretting corrosion produces only one damaged area, but it has greater wear intensity. There is disagreement in the literature on the use of the terms false brinelling and fretting corrosion,<sup>39-42</sup> since both mechanisms are caused by oscillating movements. The important difference is that false brinelling takes place in lubricated contacts, whereas fretting corrosion occurs in nonlubricated ones. Moreover, the use of the terms is made more difficult by the fact that, as the number of cycles increases, the lubricant is displaced from the contact. In this case, false brinelling can escalate to fretting corrosion.<sup>9</sup> The transition from false brinelling to fretting corrosion is shown in Figure 7. Assuming that only small oscillation amplitudes predominate and thus there is no separating lubricating film, the asperity tips of the two contact surfaces make contact. Mixed friction predominates, and the characteristic pattern of false brinelling appears as the oxide layer is worn away. The lubricant and the oxide particles are transported away



**FIGURE 6** False brinelling damage [Colour figure can be viewed at [wileyonlinelibrary.com](http://wileyonlinelibrary.com)]



**FIGURE 7** (A) Transition from false brinelling to fretting corrosion, (B) wear as a consequence of using bearing in oscillating mode, and (C) magnetite barrier and hematite depositions (based on previous studies<sup>39-42</sup>) [Colour figure can be viewed at [wileyonlinelibrary.com](http://wileyonlinelibrary.com)]

from the contact as a consequence of the oscillating movement. As the number of cycles increases, the quantity of lubricant present in the contact decreases and that of the oxide particles increases. The consequence can be that the particles form barriers that prevent any of the lubricant from flowing back. In this event, dry friction conditions prevail in the bearing. This inevitably leads to fretting corrosion and significant abrasive wear occurs as secondary damage due to adhesive wear (temporary welding of raceway and rolling element) and the particles resulting therefrom. The schematic depicted in Figure 7A can be recognized in Figure 7B,C. The high-resolution image (Figure 7C) shows that barriers have already formed as a result of this damage, and the formation of hematite is well advanced. If the wind turbine continued to be operated with these parameters, the adhesive wear and particles would promote aggressive wear. The transition from false brinelling to fretting corrosion shows the effect of the number of cycles, which is influenced by the controller.

Wear can also occur for higher  $x/2b$  ratios ( $x/2b > 1.5$ ). This wear does not exhibit the typical zones of false brinelling, however, where the outer regions of the raceway are damaged, but the inner regions are undamaged. At larger amplitudes, the whole region is usually damaged.

To explain the wear mechanisms in the contact between rolling element and raceway, a submodel of the contact was created, which allows the analysis of the occurring slip, sliding directions, and pressure. The submodel contains the ball and a raceway section of the inner and outer ring and ensures a realistic approach of the problem where the degrees of freedom are only restricted by frictional forces of the contact. A detailed description of the model, an experimental validation, and a parameter study on the influence of the bearing geometry on the frictional work density can be found in Schwack et al.<sup>22</sup>

The wear damage of a four-point contact bearing with a pitch diameter of 675 mm can be seen in Figure 8A. The pitch angle was approximately  $\pm 0.25^\circ$ , which leads to an  $x/2b$  ratio of roughly 1.5 at a pressure of 2.3 GPa. As can be seen, the damage extends over the whole contact. A more detailed analysis makes it possible to identify three sections. The greatest damage occurs in the top and bottom sections. Here, the spin with superimposed microslip is the trigger for the increased wear.<sup>22</sup> The spin occurs with all bearings having a contact angle greater than  $0^\circ$ . Circular wear can be seen in the center region. This wear is caused by microslip, which in turn is caused by the oscillation. The comparatively large pitch amplitude means the microslip increases in importance, which is also evident in the damage. Figure 8B shows the simulated friction work density,<sup>22</sup> which is the product of the friction coefficient, slip, and local pressure. Figure 9 shows exemplary slip distributions and the slip directions. The left part displays the amount of slip while the right part shows the directions of the relative slip. Areas without arrows show no relative movement. The form and intensity of the occurring wear of the aforementioned experiments coincide with the analyzed slip in Figure 9.

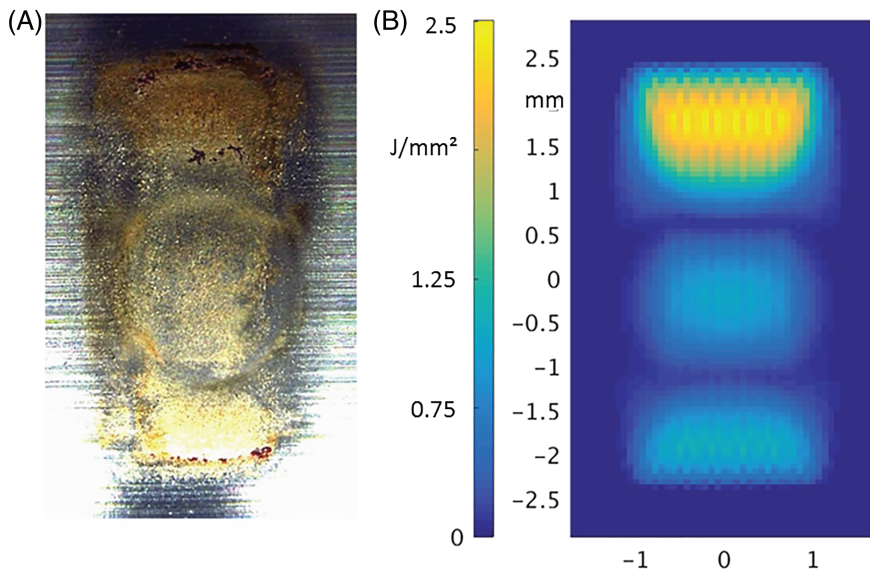
### 2.5.3 | Effect of the wind turbine controller

Now that the different damage mechanisms have been explained, the effect of the controller shall also be discussed. The operating conditions to which a rotor blade is exposed make a one-dimensional consideration of the parameters more difficult. The effects discussed here can thus serve only as an indicator.

The oscillation amplitude is crucial for the behavior of the lubricating film.<sup>43</sup> Model experiments by Maruyama et al showed that an  $x/2b > 1.5$  is necessary to ensure that a lubricating film is established.<sup>34</sup>

The oscillation frequency of the controller likewise has an impact on the occurrence of raceway fatigue or wear. Maruyama et al investigated the effect of oils and greases in oscillating applications with the aid of model experiments.<sup>34,44,45</sup> The experiments showed that the frequency had





**FIGURE 8** A, Damage from experimental investigations; B, distribution of simulated friction work density [Colour figure can be viewed at [wileyonlinelibrary.com](http://wileyonlinelibrary.com)]

no effect with  $x/2b < 1.5$ , since it was not possible for a lubricating film to be established. Above this  $x/2b$  ratio, higher frequencies result in less visible damage on the raceways. Higher  $x/2b$  ratios result in a steady rolling condition where the lubrication film thickness rises with higher rolling speeds.<sup>46</sup>

These results have only limited applicability to blade bearings. On the one hand, the reflow behavior of the lubricant used is comparable only with a limited extent. On the other hand, the experiments undertaken by Maruyama were conducted as model experiments on a ball-on-disk tribometer. The maximum contact pressure here was 0.37 GPa and the maximum rolling element speed 20 mm/s. The rolling bearing investigated here had contact pressure values of around 2 GPa, and the rolling speeds were between 50 and 125 mm/s.

The number of oscillation cycles has a significant effect on the extent of the wear. The greater the number of oscillation cycles that occur, the higher the probability that wear sets in. If a large number of oscillation cycles occur at the same contact zone, there is moreover the danger that adhesive wear takes place and particle barriers are formed, which in turn can lead to abrasive wear.

To protect the rolling bearing against wear as much as possible, it is desirable for the oscillation amplitudes to be as large as possible, for the oscillation frequency to be sufficient, and for there to be as few cycles as possible. This is inconsistent with the parameters desired for the pitch controller. To meet the aerodynamic demands and the demands imposed by tribology as well, a detailed analysis of the operating parameters that result from the controlling concept is absolutely imperative.

## 2.6 | Analysis of movement patterns

Publications on the design of IPC often draw attention to the fact that the pitch drive exhibits a higher relative activity.<sup>5,47,48</sup> The measurand for this is called the “actuator duty cycle (ADC)” and is the sum of all pitch movements. Basically, however, not every activity can be considered to be critical for damage formation, as described above. In particular, the mechanisms inducing damage to the surface are most likely to occur with oscillating movements of relatively small amplitude.

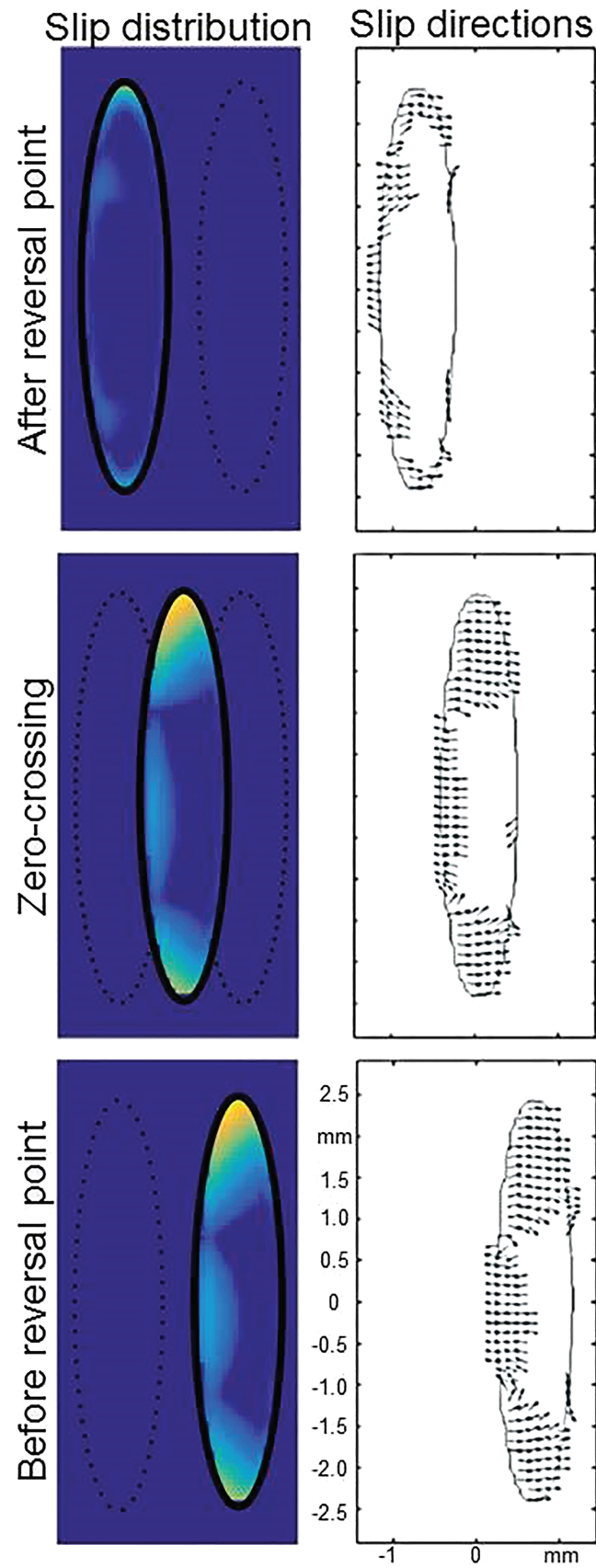
It therefore serves no purpose to sum the movements of the blade bearing, since the value thus obtained does not provide any information about the possible damage. Since the blade bearing executes oscillatory movements, it is not the sum but the individual cycles that have to be analyzed. Stammler et al described that range counting is to be preferred over rain flow counting.<sup>49</sup>

The output data of the load simulation were evaluated with the Matlab tool described in Stammler et al.<sup>49</sup> In addition to the oscillation analysis, a two-stage grouping of further values was used: Grouping the pitch angles during the cycles makes it possible to determine the extent to which cycles occur in the same value range, a subsequent grouping of the bending moment makes it possible to additionally analyze the behavior of the loads as the blade bearings move (Figure 10). The resulting bending moment  $M_{resB}$  is calculated with the aid of the torque moment  $M_{xB}$  and the thrust moment  $M_{yB}$  in accordance with Equation (3).

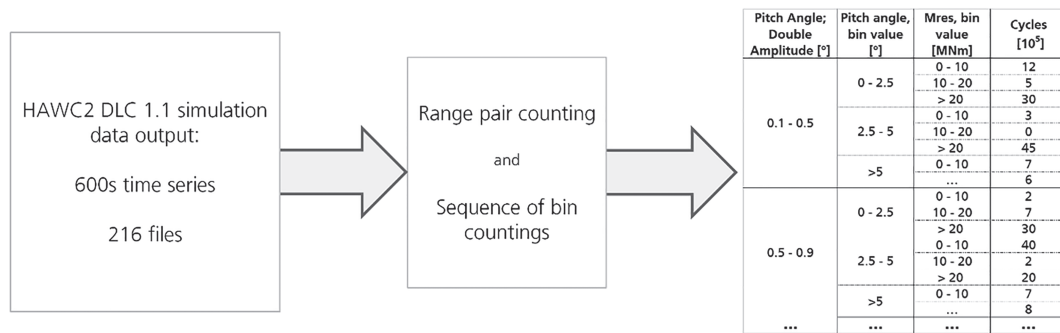
$$M_{resB} = \sqrt{M_{yB}^2 + M_{xB}^2}. \quad (3)$$

The input signal for the movement pattern analysis is the pitch angle, which is given in degrees. To estimate the probability of damage mechanisms, the ratio of the distance covered and the width of the contact area ( $x/2b$ ) provides more information, however. In Schwack et al,<sup>24</sup> the authors stated the loads of the individual rolling elements for different operating conditions for the bearing considered here. The values ranged





**FIGURE 9** Slip distributions and directions during the oscillation [Colour figure can be viewed at [wileyonlinelibrary.com](http://wileyonlinelibrary.com)]



**FIGURE 10** Cycle analysis with subsequent grouping

up to a maximum of 72.17 kN. According to Hertz,<sup>50</sup> or with the aid of approximation functions, which do not use elliptic integrals,<sup>51</sup> the dimensions of the contact area and the penetration of the bodies can be calculated.

Table 3 lists the contact area widths for load values between 30 and 80 kN; 30 kN resulting from sole pretension is assumed to be the lower boundary for the individual rolling element loads.

As can be seen in Table 3, the widths of the contact surfaces vary by a maximum of 0.832 mm between pretension and extreme loading. The bearing has a nominal diameter of 4690 mm. Assuming a rolling movement without slip, the inner ring covers twice the distance covered by the rolling element. The distance *x* covered by the rolling element is thus approximately 10 mm for every 0.5° of pitch angle.

The total distance *X* covered by each rolling element during the service life of the wind turbine can be estimated using Equation (4), where *x* is the aforementioned distance covered by the rolling element and *n* is the number of cycles.

$$X_{IPC/CPC} = x \cdot n \tag{4}$$

### 3 | RESULTS AND DISCUSSION

#### 3.1 | Load simulation

The DELs at the blade root of rotor blade 1 for the simulation with activated IPC and with deactivated IPC are presented below. To this end, IPC was switched on and off, respectively, in the parameters of the pitch controller. All other parameters were identical in both simulations. The DELs<sup>52</sup> for the four Woehler gradients *m* of 4, 8, 10, and 14 are determined for the operation in power production between cut-in and cut-out wind speed. The DELs represent an equivalent load, which leads to a figure of 10 million for the number of cycles. Since only 95% of the total service life of the turbine is considered with the simulation data of DLC1.2, the number of cycles decreases to approximately 9.5 million.

The DELs with deactivated IPC are shown in Table 4. As the friction torque of the pitch bearing was not part of the simulation, the following results do not contain *M<sub>z</sub>*. The DELs with activated IPC can be found in Table 5.

Figure 11 shows the power density spectrum of the accumulated pitch angles of all simulations in the full load region between 11 and 25 m/s, both with and without IPC. The increased power around 1P (0.16 Hertz) is clearly visible in the case of activated IPC and illustrates the increased pitch activity in this area.

**TABLE 3** Rolling element loads and contact surface width 2*b*

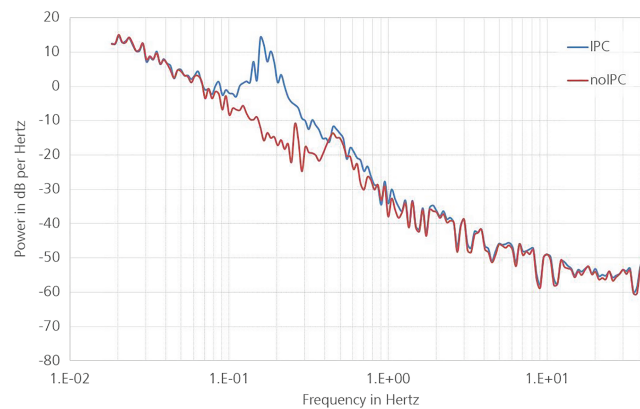
Q, kN	2 <i>b</i> , mm
30	2.112
40	2.338
50	2.518
60	2.676
70	2.816
80	2.944

**TABLE 4** DELs without IPC

m	$F_x$ , kN	$F_y$ , kN	$F_z$ , kN	$M_x$ , kN m	$M_y$ , kN m
4	563.3	1096.5	1075.0	23 488.2	22 802.0
8	541.1	838.2	847.6	18 200.5	21 928.9
10	556.2	795.7	824.1	17 413.2	22 523.5
14	592.3	751.7	825.2	16 747.6	23 848.7

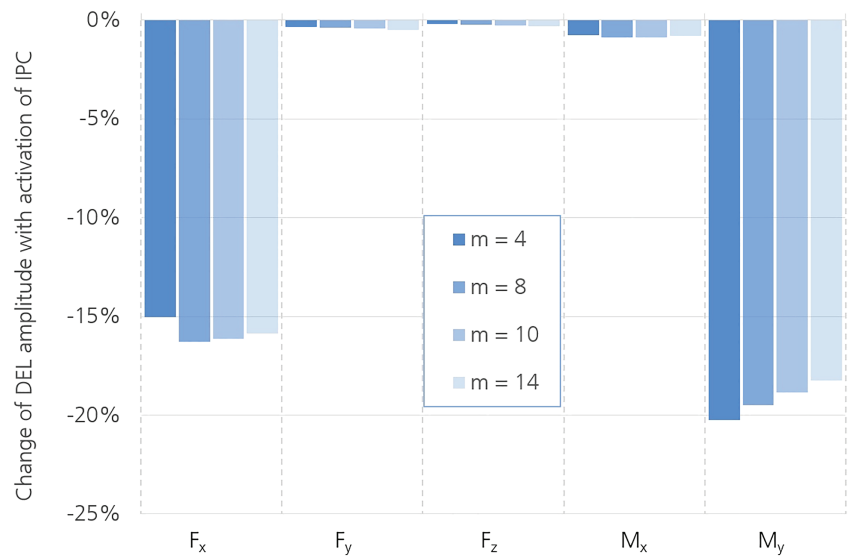
**TABLE 5** DELs with IPC

m	$F_x$ , kN	$F_y$ , kN	$F_z$ , kN	$M_x$ , kN m	$M_y$ , kN m
4	478.6	1092.7	1072.8	23 306.5	18 187.3
8	453.1	834.9	845.6	18 043.2	17 654.7
10	466.4	792.3	821.9	17 261.1	18 275.5
14	498.3	748.1	822.6	16 611.8	19 494.2

**FIGURE 11** PSD of wind speeds 11, 13, 15, 17, 23, and 25 m/s without yaw error [Colour figure can be viewed at wileyonlinelibrary.com]

The comparison of the two simulations clearly shows the effect of IPC on the loads at the blade root. The forces in all three spatial directions are sometimes significantly reduced by IPC: by only a minimal extent in the  $y$ - and  $z$ -directions, but in the  $x$ -direction by up to 16.3% for  $m = 8$ . In the three moments, the shift of the loads, which occurs because of the increased pitch activity, becomes clear. The flapwise bending moment  $M_y$  is reduced significantly by up to 20.2% for  $m = 4$ ; the edgewise moment  $M_x$  is reduced slightly.

Figure 12 uses the simulation with deactivated IPC as the reference at 100% and shows the changes brought about by the activation of the IPC.

**FIGURE 12** Change to the DELs at the blade root with IPC active [Colour figure can be viewed at wileyonlinelibrary.com]

### 3.2 | Movement patterns

Table 6 contains the results of the cycle counting for the simulation without and with IPC. The actuator duty cycle (ADC) of the pitch system increases by 4.6% to 60 141 hours when IPC is used. The increase is relatively small compared with that in other literature sources.<sup>5,53,54</sup> Moreover, the number of cycles with relatively small oscillation amplitudes (0.05-1.05°) decreases when IPC is used. This behavior can be explained from the philosophy of the controller used (cf Section 2.2): The 1P control for blade root loads leads to cycles with an oscillation amplitude of more than 1°. If IPC is active, the generator moment is reduced slightly. When CPC is used, a large number of very short angle adjustments of all blades are executed in the same operating situations, however, to keep the generator moment at the nominal moment. The slight reduction in the moment by the IPC is sufficient, however, so that a fine adjustment of all blades simultaneously is no longer required.

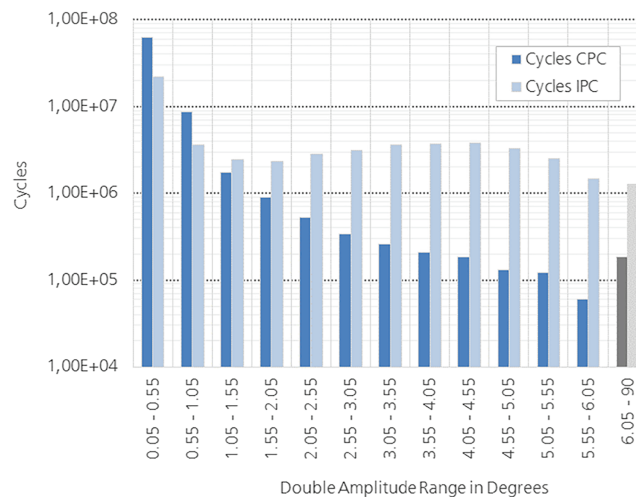
When CPC is used, every rolling element covers a distance of 381 km during the total life; in the case of IPC, this distance increases significantly to 6228 km (+1633%). The total for all cycles is  $7.53 \cdot 10^7$  when CPC is used and  $5.59 \cdot 10^7$  when IPC is used (-26%).

Figure 13 shows the cycle distribution in the direct comparison of CPC/IPC. IPC adds further cycles, particularly in the oscillation amplitude range above 1.55°. On the basis of Table 3, an amplitude of 1.55° corresponds to an  $x/2b$  ratio of 10 to 15.

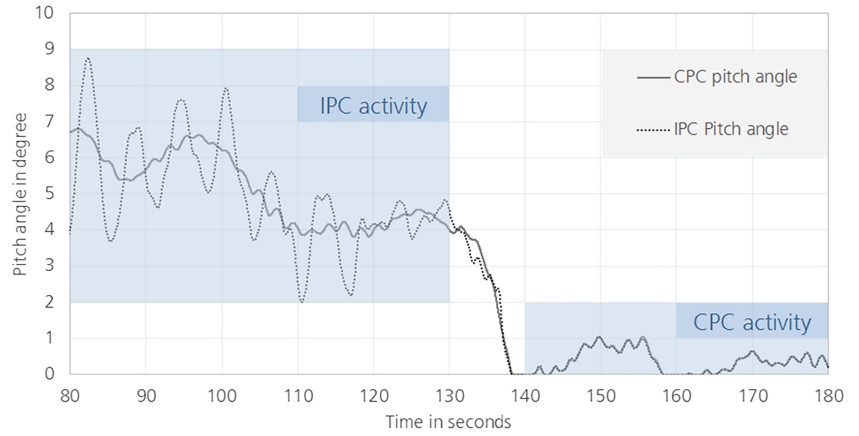
Figure 14 shows the behavior described above with the aid of the light blue highlighted areas, in which IPC-typical (80-130 s) and CPC-typical (140-180 s) movements are executed. The IPC is only active above a collective pitch angle of 2.3°, as such the behavior of IPC and CPC match between 140 and 180 s. The greater number of movements with small oscillation amplitude with the CPC controller can be clearly seen in the range from 80 to 130 seconds.

**TABLE 6** Cycle counting results for 0° to 90°

Double Amplitude Range, °	CPC		IPC	
	Number of Full Cycles	Mean Frequency, Hz	Number of Full Cycles	Mean Frequency, Hz
0.05-0.55	$62.00 \cdot 10^6$	0.50	$22.00 \cdot 10^6$	0.59
0.55-1.05	$8.60 \cdot 10^6$	0.27	$3.65 \cdot 10^6$	0.36
1.05-1.55	$1.73 \cdot 10^6$	0.14	$2.41 \cdot 10^6$	0.25
1.55-2.05	$0.90 \cdot 10^6$	0.10	$2.31 \cdot 10^6$	0.22
2.05-2.55	$0.53 \cdot 10^6$	0.09	$2.85 \cdot 10^6$	0.19
2.55-3.05	$0.34 \cdot 10^6$	0.08	$3.15 \cdot 10^6$	0.18
3.05-3.55	$0.26 \cdot 10^6$	0.07	$3.57 \cdot 10^6$	0.17
3.55-4.05	$0.21 \cdot 10^6$	0.07	$3.72 \cdot 10^6$	0.17
4.05-4.55	$0.18 \cdot 10^6$	0.06	$3.78 \cdot 10^6$	0.17
4.55-5.05	$0.13 \cdot 10^6$	0.05	$3.25 \cdot 10^6$	0.17
5.05-5.55	$0.12 \cdot 10^6$	0.06	$2.51 \cdot 10^6$	0.16
5.55-6.05	$0.06 \cdot 10^6$	0.05	$1.48 \cdot 10^6$	0.16
6.05-90	$0.19 \cdot 10^6$	0.04	$1.25 \cdot 10^6$	0.15



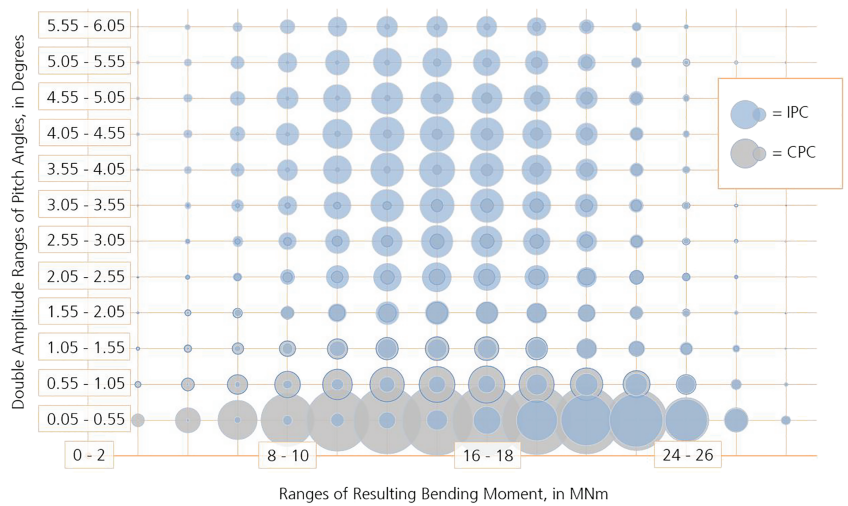
**FIGURE 13** Number of cycles CPC/IPC in comparison for all oscillation amplitude ranges [Colour figure can be viewed at [wileyonlinelibrary.com](http://wileyonlinelibrary.com)]



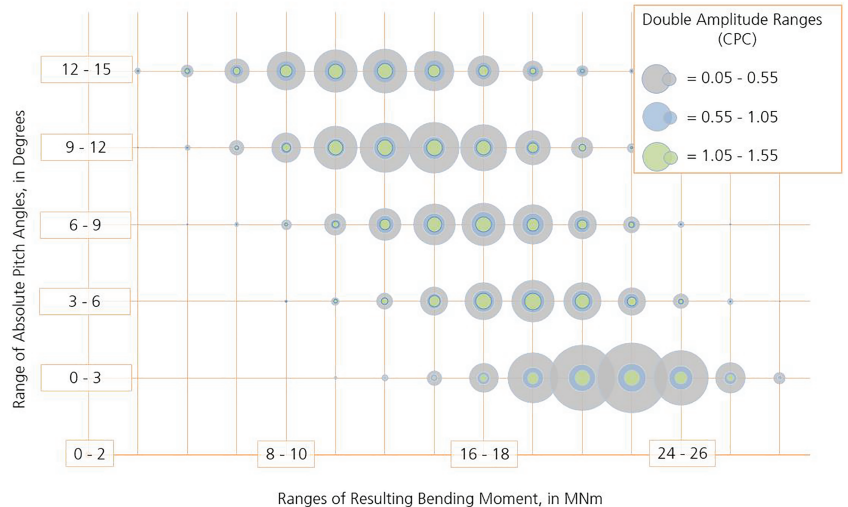
**FIGURE 14** Blade bearing movement pattern with and without IPC for an average wind speed of 11 m/s, yaw = 0° [Colour figure can be viewed at wileyonlinelibrary.com]

Figure 15 shows the grouping of the resultant bending moment  $M_{resB}$ , divided up into the classes of cycle counting of the pitch angle for one of the rotor blades. The position of the individual circles gives the pitch angle and moment classes, the diameter corresponds to the absolute time spent in the respective class. The larger the circle diameter, the longer the time spent.

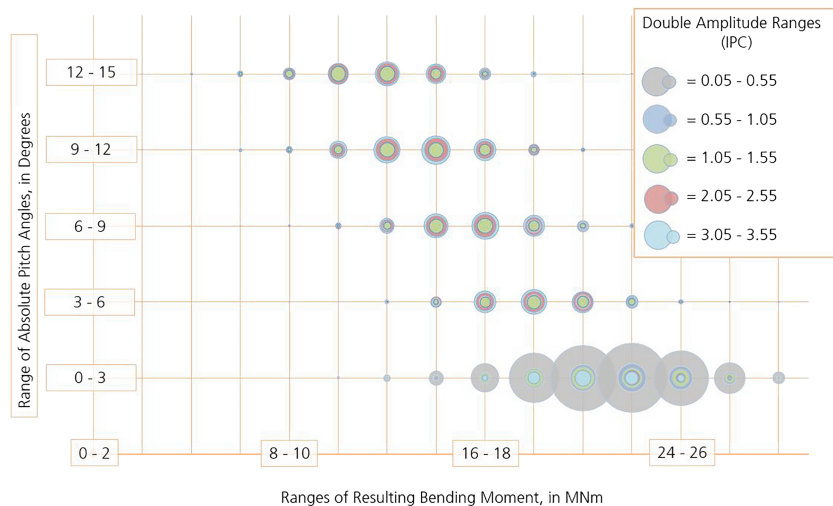
In the case of CPC, it turns out that the movement cycles are distributed relatively uniformly over the classes of the bending moment and are dominated by small pitch angles up to 1.05°. This results from the fact that all three rotor blades are controlled simultaneously for the generator



**FIGURE 15** Grouping of the resulting bending moment for oscillation amplitude ranges up to 6.05° [Colour figure can be viewed at wileyonlinelibrary.com]



**FIGURE 16** Incremental grouping of pitch angle and resulting bending moment for CPC and oscillation amplitude ranges up to 1.55° [Colour figure can be viewed at wileyonlinelibrary.com]



**FIGURE 17** Incremental grouping of pitch angle and resulting bending moment for IPC and selected oscillation amplitude ranges up to  $3.55^\circ$  [Colour figure can be viewed at [wileyonlinelibrary.com](http://wileyonlinelibrary.com)]

torque. In the case of IPC, it can be seen that movements with slightly larger pitch angles ( $2.05^\circ$  and above) are more likely to occur with smaller bending moments, as IPC reduces the thrust moment.

Further information on the controller behavior is provided by cycle counting with subsequent incremental grouping. This is shown in Figures 16 and 17. Here, the cycles were first evaluated as for Figure 13, before the absolute pitch angle was grouped. The cycle counting provides relative values for the change in the pitch angle and no absolute values; this is achieved only by the grouping. After the cycle counting and the grouping of the pitch angle, the bending moment is grouped. The results are shown in Figure 16 for CPC and Figure 17 for IPC.

As described in the previous explanations, CPC operates with smaller pitch angles, which explains why Figure 16 shows only three classes of oscillation amplitudes up to  $1.55^\circ$ . At higher absolute pitch angles, smaller moments are more likely to occur, because above the nominal wind speed all blades are pitched, and this results in a reduction in the proportion of the thrust moment. The difference between IPC and CPC is also evident in the regions of higher absolute pitch angles. Here, IPC has a lower number of cycles with smaller oscillation amplitudes up to  $1.55^\circ$ , and a higher number of cycles with larger oscillation amplitudes. Oscillation amplitudes above  $3.55^\circ$  were not included in Figure 17 for reasons of clarity. Figure 15 leads to the conclusion that these exhibit a behavior similar to that of the oscillation amplitudes shown, however.

## 4 | CONCLUSIONS

This paper considers the consequences of using an IPC controller for the rotor blade bearing. To this end, simulations of the reference turbine IWT-7.5-164 were executed and evaluated. The evaluation comprised the fatigue loads of the structure and the movement patterns and loads of the rotor blade bearing.

Previous publications on IPC showed that IPC reduces the fatigue loads and increases the general pitch activity. The results of this work agree with these findings. The increase in the proportion of time spent on the pitch activity of 4.6% is lower than that in other publications in this field. The reason for this difference is the layout of the IPC of the IWT-7.5-164, which is only active above pitch angles of  $2.3^\circ$  set by the CPC in comparison with other IPCs that are active at all CPC set angles. The larger oscillation amplitudes for IPC result in a significant increase in the total distance covered by each rolling element from 381 km to 6228 km during the service life of a wind turbine.

Since mechanisms that induce damage on the surface of the bearing raceways depend on the oscillation amplitudes and loads of the oscillating movements, a cycle analysis was also conducted. This showed that the IPC analyzed in this study had more cycles than CPC above an oscillation amplitude of  $1.55^\circ$  and lesser cycles at amplitude of below  $0.55^\circ$ . The ratio  $x/2b$ , which is important for the damage mechanisms in the blade bearing, is 10 to 15 for an amplitude of  $1.55^\circ$  (depending on the rolling element load). It can therefore be assumed that the IPC investigated here does not lead to additional false brinelling on the bearing raceways; this occurs more frequently with smaller oscillation amplitudes. Furthermore, the mean values of the oscillation vary by a relatively large amount. This reduces the probability of surface wear in general, since it is always different areas of the raceway that are in contact with the rolling elements. The high number of cycles for any  $x/2b$  ratio still imposes a significant risk for surface-induced damage modes.

The increase in the distance covered makes the assessment of the rolling contact fatigue clear: For the controller of the IWT7.5-164, the risk of rolling contact fatigue is increased by the use of IPC. It is not possible to give a final assessment of the risk of wear occurring on the basis of the current state of our knowledge. The probability of false brinelling occurring is reduced by the larger oscillation amplitudes. The probability of fretting corrosion occurring is reduced due to the fact that the mean values of the oscillations is different. It is not possible to provide a final assessment of the extent to which the kinetic parameters (load, rolling speed, oscillation amplitudes, temporal sequence) of the oscillations executed are conducive to fretting corrosion. However, the wear risk gets smaller with the application of IPC.



To remove these doubts, further research work, particularly tests with different kinetic parameters, is necessary.

## ACKNOWLEDGEMENTS

The present work was carried out with the project “HAPT – Highly Accelerated Pitch Bearing Tests.” The project funding by the German Federal Ministry for Economic Affairs and Energy is kindly acknowledged. The authors would also like to thank Marcus Wiens for his contribution to the IPC documentation.

## ORCID

Matthias Stammler  <https://orcid.org/0000-0003-1874-1344>

## REFERENCES

- Burton T. *Wind Energy Handbook*. 2nd ed. Chichester, New York: Wiley; 2011.
- Laks JH, Pao LY, Wright AD. Control of wind turbines: past, present, and future, in *2009 American Control Conference*. 2009 American Control Conference, 10.06.2009-12.06.2009, St. Louis, MO, USA. IEEE, 2009. pp. 2096–2103.
- Bossanyi EA. Individual blade pitch control for load reduction. *Wind Energy*. 2003;6(2):119-128.
- Barlas TK, van Kuik GAM. Review of state of the art in smart rotor control research for wind turbines. *Prog Aerosp Sci*. 2010;46(1):1-27.
- Bottasso CL, Croce A, Riboldi CED, Salvetti M. Cyclic pitch control for the reduction of ultimate loads on wind turbines. *J Phys: Conf Ser*. 2014;524:12063.
- Aguirrebeitia J, Plaza J, Abasolo M, Vallejo J. General static load-carrying capacity of four-contact-point slewing bearings for wind turbine generator actuation systems. *Wind Energ*. 2013;16(5):759-774.
- Harris TA, Kotzalas MN. *Rolling bearing analysis*. 5th ed. Boca Raton: CRC, Taylor & Francis; 2007.
- DIN ISO 281. *Wälzlager - Dynamische Tragzahlen und nominelle Lebensdauer (ISO 281:2007)*, DIN ISO, Berlin; 2010.
- Schwack F, Byckov A, Bader N, Poll G. Time-dependent analyses of wear in oscillating bearing applications. *2017 STLE Annual Meeting*, Atlanta; 2017.
- Grebe M, Feinle P, Blaškovitš P. Failure of roller bearings without macroscopic motion—influence of the pivoting angle on the contact mechanics and the wear mechanisms in the contact between roller and raceway, in *Tribology - industrial and automotive lubrication* (ed W.J. Bartz), Techn. Akad. Esslingen, Ostfildern; 2014.
- Stammler M, Poll G. Schadensmechanismen in Rotorblattlagern. *GfT - Reibung, Schmierung und Verschleiss*, Göttingen; 2014.
- Njiri JG, Söffker D. State-of-the-art in wind turbine control: trends and challenges. *Renew Sustain Energy Rev*. 2016;60:377-393.
- Shan M, Jacobsen J, Adelt S. Field testing and practical aspects of load reducing pitch control systems for a 5 MW offshore wind turbine, in *European Wind Energy Conference & Exhibition (EWEC 2013): Vienna, Austria, 4-7 February 2013*. Curran, Red Hook, NY, 2014; pp. 1551–1560.
- Schwack F, Stammler M, Poll G, Reuter A. Comparison of life calculations for oscillating bearings considering individual pitch control in wind turbines. *J Phys: Conf Ser*. 2016;753:112013.
- Houper L. bearing life calculation in oscillatory applications. *Tribol Trans*. 1999;42(1):136-143.
- Harris T, Rumbarger JH, Butterfield CP. *Wind Turbine Design Guideline DG03: Yaw and Pitch Rolling Bearing Life*. Colorado: Golden; 2009.
- Nam JS, Park YJ, Chang HS. Dynamic life prediction of pitch and yaw bearings for wind turbine. *J Mech Sci Technol*. 2016;30(1):249-256.
- Stammler M, Schwack F, Bader N, Reuter A, Poll G. Friction torque of wind-turbine pitch bearings—comparison of experimental results with available models. *Wind Energy Sci*. 2018;3(1):97-105.
- Han JW, Nam JS, Park YJ, Lee GH, Nam YY. An experimental study on the performance and fatigue life of pitch bearing for wind turbine. *J Mech Sci Technol*. 2015;29(5):1963-1971.
- Stammler M, Reuter A. Blade bearings: damage mechanisms and test strategies. *Conference for Wind Power Drives*, Aachen; 2015.
- FVA. *Größeneinfluss Wälzlagerverschleiß: Einfluss der Wälzlager-Baugröße auf das Verschleißverhalten von Wälzlagern*, Frankfurt, *Forschungsvorhaben 327/III*; 2011.
- Schwack F, Prigge F, Poll G. Finite element simulation and experimental analysis of false brinelling and fretting corrosion. *Tribol Int*. 2018;126:352-362.
- Bleich O, Meng F, Daniele E, Thomas P, Popko W. *IWES WIND TURBINE IWT-7.5-164 REV. 2.5*, Fraunhofer IWES; 2016.
- Schwack F, Stammler M, Flory H, Poll G. Free contact angles in pitch bearings and their impact on contact and stress conditions. *WindEurope Conference, Hamburg*; 2016.
- Larsen TJ, Hansen AM *How 2 HAWC2, the User's Manual*, Risø National Laboratory, Roskilde, 1597; 2015.
- Bak C, Zahle F, Bitsche R, et al. Description of the DTU 10 MW reference wind turbine. <http://dtu-10mw-rwt.vindenergi.dtu.dk>.
- IEC 61400-1. *Wind turbines—part 1: design requirements*, IEC, Geneva; 2005.
- Hayman GJ, Buhl M. *Mlife user's guide for version 1.0*; 2012.
- Dowson D, Ehret P. Past, present and future studies in elastohydrodynamics. *Proc Inst Mech Eng Part J: J Eng Tribol*. 1999;213(5):317-333.
- Ioannides E, Harris TA. A new fatigue life model for rolling bearings. *J Tribol*. 1985;107(3):367.
- DIN. *DIN ISO 281 - Dynamic Load Ratings and Rating Life*. Berlin: Beuth Verlag; 2007.



32. Sadeghi F, Jalalahmadi B, Slack TS, Raje N, Arakere NK. A review of rolling contact fatigue. *J Tribol*. 2009;131(4):041403.
33. Lundberg G, Palmgren A. *Dynamic Capacity of Rolling Bearings*. 196 Stockholm: Generalstabens Litografiska Anstalts Förl.; 1947.
34. Maruyama T, Saitoh T. Oil film behavior under minute vibrating conditions in EHL point contacts. *Tribol Int*. 2010;43(8):1279-1286.
35. Almen JO. Lubricants and false brinelling of ball and roller bearing. *J Mech Eng*. 1937;59:415-422.
36. Godfrey D. A Study of fretting wear in mineral oil. *Lub Eng*. 1956;12:37-42.
37. Mindlin RD. Compliance of elastic bodies in contact. *J Appl Mech*. 1949;16:259-268.
38. Godfrey D. Iron oxides and rust (hydrated iron oxides) in tribology. *Lubri Eng*. 1999;55:33-37.
39. Errichello R. True Brinelling, & Fretting corrosion—what's the difference? *GEARTECH*; 2014.
40. Godfrey D. Fretting corrosion or false brinelling? *Tribol Lubri Technol*. 2003;59:28-29.
41. Errichello R. Another perspective: false brinelling and fretting corrosion. *Tribol Lubri Technol*. 2004;60:34-36.
42. Grebe M, Feinle P. Brinelling, false-brinelling, "false" false-brinelling. In: *Reibung, Schmierung und Verschleiss: Forschung und praktische Anwendungen*. Aachen: Tribologie-Fachtagung. GFT; 2006:49/1-49/11.
43. Hamrock BJ, Dowson MD. Isothermal elastohydrodynamic lubrication of point contacts: part III—fully flooded results. *J Lubri Tribol*. 1977;1977:264-276.
44. Zhou ZR, Nakazawam K, Zhu MH, Maruyama N, Kapsa P, Vincent L. Progress in fretting maps. *Tribol Int*. 2006;2006(39):1068-1073.
45. Maruyama T, Saitou T, Yokouchi A. Differences in mechanisms for fretting wear reduction between oil and grease lubrication. *Tribol Trans*. 2016;60:497-505.
46. Lubrecht AA, Venner CH, Colin F. Film thickness calculation in elasto-hydrodynamic lubricated line and elliptical contacts: the Dowson, Higginson, Hamrock contribution. *Proc Inst Mech Eng Part J: J Eng Tribol*. 2009;223(3):511-515.
47. Stol K Balas M. Periodic disturbance accommodating control for speed regulation of wind turbines, in *ASME 2002 Wind Energy Symposium*, January 14-17, 2002, Reno, Nevada, USA, 2002; pp. 310-320.
48. Riboldi CE. On the optimal tuning of individual pitch control for horizontal-axis wind turbines. *Wind Eng*. 2016;40(4):398-416.
49. Stammeler M, Reuter A, Poll G. Cycle counting of roller bearing oscillations - case study of wind turbine individual pitching system. *Renewable Energy Focus*. 2017; 25:40-47.
50. Hertz HR. Über die Berührung fester elastischer Körper. *J Reine Angew Math*. 1881;92:156-171.
51. Houpert L. An engineering approach to Hertzian contact elasticity—part I. *J Tribol*. 2001;123(3):582.
52. Stammeler M, Reuter A, Poll G. Cycle counting of roller bearing oscillations—case study of wind turbine individual pitching system. *Renew Energy Focus*. 2018;25:40-47.
53. Larsen TJ, Madsen HA, Thomsen K. Active load reduction using individual pitch, based on local blade flow measurements. *Wind Energy*. 2005;8(1):67-80.
54. Barlas TK, van Kuik GAM. State of the art and perspectives of smart rotor control for wind turbines. *J Phys*. 2007;75:012080.

**How to cite this article:** Stammeler M, Thomas P, Reuter A, Schwack F, Poll G. Effect of load reduction mechanisms on loads and blade bearing movements of wind turbines. *Wind Energy*. 2020;23:274-290. <https://doi.org/10.1002/we.2428>